Available online at www.sciencedirect.com
ScienceDirect
Journal of Magnetic Resonance 186 (2007) 176–181
JMR Journal of Magnetic Resonance
www.elsevier.com/locate/jmr

Relaxation of protons by radicals in rotationally immobilized proteins

Jean-Pierre Korb [a], Galina Diakova [b], Yanina Goddard [b], Robert G. Bryant [b,*]

[a] *Physique de la Matière Condensée, Ecole Polytechnique, CNRS, 91128 Palaiseau, France*
[b] *Chemistry Department, University of Virginia, P.O. Box 400319, Charlottesville, VA 22904-4319, USA*

Received 22 November 2006; revised 29 January 2007
Available online 13 February 2007

Abstract

Proton spin–lattice relaxation by paramagnetic centers may be dramatically enhanced if the paramagnetic center is rotationally immobilized in the magnetic field. The details of the relaxation mechanism are different from those appropriate to solutions of paramagnetic relaxation agents. We report here large enhancements in the proton spin–lattice relaxation rate constants associated with organic radicals when the radical system is rigidly connected with a rotationally immobilized macromolecular matrix such as a dry protein or a cross-linked protein gel. The paramagnetic contribution to the protein–proton population is direct and distributed internally among the protein protons by efficient spin diffusion. In the case of a cross-linked-protein gel, the paramagnetic effects are carried to the water spins indirectly by chemical exchange mechanisms involving water molecule exchange with rare long-lived water molecule binding sites on the immobilized protein and proton exchange. The dramatic increase in the efficiency of spin relaxation by organic radicals compared with metal systems at low magnetic field strengths results because the electron relaxation time of the radical is orders of magnitude larger than that for metal systems. This gain in relaxation efficiency provides completely new opportunities for the design of spin–lattice relaxation based contrast agents in magnetic imaging and also provides new ways to examine intramolecular protein dynamics.

Keywords: Paramagnetic relaxation; MRD; Relaxation dispersion; Relaxation agent

1. Introduction

Magnetic relaxation agents or contrast agents for clinical magnetic imaging applications are generally based on soluble chelate complexes of gadolinium(III) that provide one or more coordination positions for labile water molecules that carry the effects of the paramagnetic center to the total water population by chemical exchange of labile protons or water molecules [1–3]. In most cases, the relaxation efficiency of these compounds is limited by the short electron spin–lattice relaxation times in the range of tens to hundreds of picoseconds, which in turn defines the concentration range where these compounds may be used as practical contrast agents [4–11]. MRI contrast agents currently in use are generally soluble extracellular and blood-pool agents; however, targeting to provide specific anatomical or biochemical information will necessarily involve binding of an agent to a cell surface site or a specific macromolecular matrix [4,12,13]. For the relaxation agents presently used, the conjugation of the agent with a macromolecule like a protein causes only a minor increase in the water–proton relaxation rate because of the limitations imposed by short electron–spin relaxation times of the metal center [6] and possibly rapid segmental reorientation about a tether [14]. Conjugation of organic radicals to soluble proteins generally produces small effects in the water–proton relaxation that are related to the rapid modulation of the electron–nuclear coupling by relative translational diffusion [15–17]. The relative translational diffusion constant is dominated by the mobile water; therefore, relaxation efficiency is severely limited, and little is gained by attaching the radical to a large macromolecule. Recent work on metalloprotein conjugates has shown, however, that in the case that the paramagnetic protein centers are strongly immobilized, the electron–spin relaxation rate constants

* Corresponding author. Fax: +1 434 924 3567.
E-mail address: rgb4g@virginia.edu (R.G. Bryant).

1090-7807/$ - see front matter © 2007 Elsevier Inc. All rights reserved.
doi:10.1016/j.jmr.2007.02.006

may increase dramatically, with a consequent increase in the spin–lattice relaxation rate constant of the coupled protons [14]. Further, in the case of a rotationally immobilized protein, which is magnetically a solid in the sense that the proton–proton dipolar couplings are not averaged, the efficient spin diffusion in the macromolecule matrix provides a fundamentally different mechanism for efficient distribution of the effects of the paramagnetic center to other nuclear spins, water protons in particular [18–21].

We report here magnetic relaxation dispersion, MRD, experiments on paramagnetic protein systems where the electron has a long spin–lattice relaxation time, T_{1e}, and where the protein is rotationally immobilized. The purpose is to provide a model for targeted relaxation agents where the target is not a freely rotating soluble solute. These experiments show that the relaxation efficiency of organic radicals may be greatly enhanced by careful control of the local dynamics of the paramagnetic center in a proton rich rigid matrix and that there may be fundamentally new ways to design contrast agents for applications to magnetic resonance imaging. We study bovine serum albumin, lyophilized, and in gels because this system is an excellent model for the relaxation in tissue [22]; lyophilization provides an example of the complete protein spin system where the local motions of the radical are quenched along with most side-chain motions [23].

2. Experimental

Bovine serum albumin (Fraction V) was obtained from Sigma (St. Louis, MO, USA), potassium phosphate monobasic and sodium hydroxide were obtained from Mallinckrodt Baker, Inc. (Paris, Kentucky, USA), acetonitrile from Fisher Scientific (Fair Lawn, NJ USA), 3-(2-iodoacetamido)-PROXYL from Sigma–Aldrich (St. Louis, MO, USA), 4-maleimido-TEMPO from Aldrich Chem. Co. (Milwaukee, WI, USA). BSA was purified by dialysis against four changes of filtered deionized water, and then lyophilized to constant weight.

BSA (1.12 g) was dissolved in 20 mL of 50 mM phosphate buffer at pH 8.5 and the solution divided in half. Iodoacetamido-PROXYL dissolved in 0.5 mL of acetonitrile and 1.0 mL of phosphate buffer was added to one portion of the BSA solution to provide a 1:1 mole ratio of spin label to protein; one equivalent of a similar 4-maleimide-TEMPO solution was added to the second half of the BSA solution and both reaction mixtures were incubated at ambient laboratory temperature over night. Each modified BSA sample was dialyzed against four changes of deionized water and then lyophilized to constant weight. The ratio between protein and spin-label in each of these two samples was found to be 1:0.6 by ESR spectroscopy. The paramagnetic proteins were transferred to individual 10 mm sample tubes, and sealed with gas-tight caps.

Paramagnetic protein gels (protein content ~15% weight/volume) were prepared in 10 mm sample tube by dissolving ~153–156 mg of the dry paramagnetic protein conjugate in 0.9 ml water and adding 0.1 ml of 25% aqueous glutaraldehyde solution at laboratory temperature. Gels formed within 10 min.

NMR experiments were conducted at 25 °C using a Stelar Spinmaster Fast Field Cycling NMR spectrometer FFC 2000 (Mede, Italy) in the magnetic field interval corresponding to proton Larmor frequencies from 0.01 to 30 MHz. Relaxation rate constants for all samples were measured using automated acquisition protocols with the proton detection frequency of 15.8 MHz and a polarization field of 30 MHz. CW EPR spectroscopy measurements were conducted using a Varian E-line 102 Series X-band spectrometer equipped with a microwave Miteq preamplifier (Hauppaugue, NY, USA) and a Loop Gap Resonator (Medical Advances Inc., Milwaukee, WI, USA). Data collection and analysis were carried out using *Labview* software provided by C. Altenbach and W. Hubbell (UCLA). Spin labeled protein solutions were placed in round borosilicate glass tubes with a 0.6 mm I.D. (VitroCom Inc., Mountain Lakes, NJ, USA). All spectra were collected at a microwave power of 2.0 mW and 1.0 G modulation amplitude. Calibration plots were obtained using the integrated intensities of EPR absorption signals from seven different concentrations of iodoacetamido-PROXYL and maleimido-TEMPO dissolved in acetonitrile and phosphate buffer.

The electron relaxation time constants for dry spin-labeled BSA were measured using a Bruker (Bellerica, MA, USA) Elexsys E 580 spectrometer that operates at 9.6 GHz. The console was equipped with a traveling wave tube amplifier (TWT) capable of producing 1 kW microwave pulses. The dielectric resonator was detuned to decrease quality factor, Q, to a value less than 200. Samples were placed in round quartz capillaries with a 1.5 mm ID (VitroCom, Inc., Mountain Lakes, NJ, USA). The spin–spin relaxation time, T_2, was measured by monitoring two pulse echo decay: $2\pi/3$–τ–$2\pi/3$–t–AQC–RD. The spin-lattice relaxation time constant was measured using an inversion recovery with echo detection pulse sequence, π–τ–$\pi/2$–t–π–t–AQC–recycle delay. The $\pi/2$ pulse length was 16 ns.

3. Results and discussion

The magnetic relaxation dispersion profile at 302 K for lyophilized diamagnetic and spin-labeled paramagnetic bovine serum albumin is shown in Fig. 1. An interesting feature of the relaxation profile of an immobilized protein system is the series of quadrupole peaks between 0.5 and 5 MHz, which arise from the coupling of protons bonded directly to amide nitrogen atoms [23]. These peaks occur when the proton resonance frequency matches one of the transition frequencies of ^{14}N, which are dominated by the interaction of the nitrogen nuclear electric quadrupole moment with the electric field gradient at the site of the ^{14}N nucleus. Due to electrical asymmetry at the nitrogen

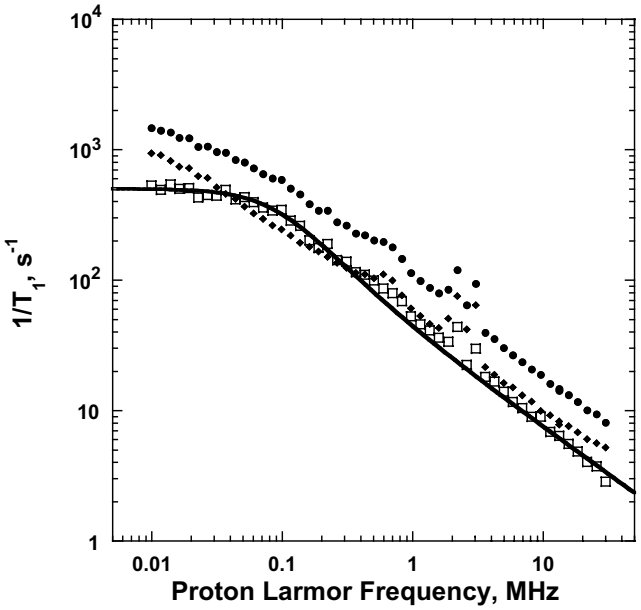

Fig. 1. The proton spin–lattice relaxation rate constant for dry bovine serum albumin covalently labeled with 0.6 equivalents of iodoacetamido-PROXYL spin label as a function of the magnetic field strength reported as the proton Larmor frequency. (●) the total relaxation rate for the paramagnetic protein; (♦) the relaxation rate constants for the unlabeled diamagnetic protein; (□) the paramagnetic relaxation rate contribution obtained by subtraction of the diamagnetic relaxation rate constants from the total relaxation rate constants. Data were obtained at 302 K on dry lyophilized protein. The solid line represents the best fit to Eq. (9) with the $T_{1e} = 1.7\ \mu s$, $b = 0.72$, and $D = 7.2 \times 10^6\ (s^{-1})^{b+1}$, where $D = 3C\pi d_S \frac{k_B T}{\hbar}\left(1+\frac{1}{2^b}\right)\Omega_{\parallel}^{b-2}\overline{M}_{2H}\frac{N_e}{N_H}\frac{\gamma_S^2}{\gamma_I^2}$. As shown in earlier [18] perpendicular vibrational modes are quenched in dry protein systems.

nucleus, there are three distinct transitions in the protein backbone ^{14}N system to which the protons may couple.

Previous studies of the proton spin–lattice relaxation rate constants in diamagnetic rotationally immobilized proteins have shown that the frequency dependence of the relaxation rate constant is a power law, physical origin of which can be related to a spin-phonon-like relaxation mechanism [18]:

$$\frac{1}{T_{1,dia}} = \overline{M}_{2H} \cdot \left[4\pi d_S \frac{k_B T}{\hbar}\left\{\frac{3}{4}\left(1+\frac{1}{2^b}\right)\Omega_{\parallel}^{b-2} + \frac{1}{6}\left(\frac{7}{2}+\frac{1}{2^b}\right)\Omega_{\perp}^{b-2}\right\}\frac{1}{\omega^b}\right] \quad (1)$$

where $\omega = \omega_0 + \omega_D$, ω_D is the local proton dipolar field strength, ω_0 is the Larmor frequency, T is the absolute temperature, k_B is Boltzmann constant, $\overline{M}_{2H}$ is the averaged second moment of protein protons, which can be measured directly from the time decay of the free precession signal [24], $\hbar\Omega_{\parallel}$ and $\hbar\Omega_{\perp}$ are the energy for the vibrational transition parallel and perpendicular to the protein backbone that are approximated by the amide(II) longitudinal vibrational mode at 1560 cm^{-1} and the perpendicular mode at 200 cm^{-1} [18,25]. The exponent in the power law, $b = 3 - 2\frac{d_S}{d_f} - d_S$, is related by the relaxation theory to a spectral dimension, d_s that characterizes the dimensionality of the disturbance propagation, and fractal dimension, d_f, which describes the distribution of protons in space.

The experimental data for the dry diamagnetic BSA were subtracted from the observed relaxation rate constants for the paramagnetic protein to obtain the paramagnetic contribution, which is shown as open squares in Fig. 1. The high field portion of the MRD profile for the paramagnetic contribution is described by a power law in the Larmor frequency as observed previously [14]; however, below 0.2 MHz, the paramagnetic contribution is independent of magnetic field strength. The relaxation dispersion is similar to that reported for strongly immobilized metal complexes on proteins [14] except that the onset of the plateau occurs at much lower frequency than for metalloprotein systems studied to date. In addition, the magnitude of the low-field paramagnetic contribution to the protein–proton relaxation rate constant is large, approximately 1000 s^{-1}, compared with approximately 100 for 1:1 metal:protein based systems. This dramatic relaxation rate increase occurs because the nitroxide-electron spin-lattice relaxation time in the dry spin-labeled protein is longer than the electron relaxation time in the similar modified metalloprotein systems.

To describe the paramagnetic contribution to the protein relaxation rate constant, one has to consider a classical correlation function, $G(\tau)$, that fulfills the following requirements:

(i) As $\tau \to 0$, the correlation function should converge to a constant value [26,27], $G(0) = 1$;
(ii) On a short time scale, on the order of $\Omega_{\parallel}^{-1}$, $\tau \sim \tau_{uf}$, where τ_{uf} is a characteristic correlation time for the high frequency fluctuation, the correlation function should behave as a power law, $G(\tau) \propto \frac{1}{(|\tau|/\tau_{uf})^{1-b}}$, characteristic of dipolar relaxation due to effects of localized dynamical disturbances;
(iii) On a timescale the order of the electron spin–lattice relaxation time, $\tau \sim T_{1e}$, where $T_{1e} \gg \tau_{uf}$, the experimentally observed cut-off should be included in the correlation function, $G(\tau) \propto \frac{\exp(-\frac{|\tau|}{T_{1e}})}{|\tau/\tau_{uf}|^{1-b}}$.

Mathematically all of the requirements listed above can be expressed in the following reduced (dimensionless) correlation function:

$$G(\tau) = \frac{1}{\left(\frac{1}{\tau_{uf}} - \frac{1}{T_{1e}}\right)}\left[1 + \left(\frac{|\tau|}{\tau_{uf}}\right)^b\right]\left(\frac{e^{-\frac{|\tau|}{T_{1e}}} - e^{-\frac{|\tau|}{\tau_{uf}}}}{|\tau|}\right). \quad (2)$$

The reduced spectral density for the paramagnetic contribution is then obtained by calculating the cosine Fourier transform of Eq. (2):

$$J_{\text{para}}(\omega) = 2\sqrt{\frac{2}{\pi}}\frac{\tau_{\text{uf}}^{1-b}T_{1\text{e}}}{T_{1\text{e}}-\tau_{\text{uf}}} \times \left\{ \begin{array}{l} \Gamma(b)\left[T_{1\text{e}}^{b}\frac{\cos[b\arctan(\omega T_{1\text{e}})]}{\left(1+\omega^2T_{1\text{e}}^2\right)^{b/2}} - \tau_{\text{uf}}^{b}\frac{\cos[b\arctan(\omega\tau_{\text{uf}})]}{\left(1+\omega^2\tau_{\text{uf}}^2\right)^{b/2}}\right] + \\ \frac{\tau_{\text{uf}}^{b}}{2}\left[\log\left(\frac{T_{1\text{e}}^2}{\tau_{\text{uf}}^2}\right) + \log\left(\frac{1+\omega^2\tau_{\text{uf}}^2}{1+\omega^2T_{1\text{e}}^2}\right)\right] \end{array} \right\}. \tag{3}$$

When $T_{1\text{e}} \gg \tau_{\text{uf}}$, Eq. (3) can be greatly simplified:

$$J_{\text{para}}(\omega) = 2\sqrt{\frac{2}{\pi}}\Gamma(b)\tau_{\text{uf}}^{1-b}T_{1\text{e}}^{b}\frac{\cos[b\arctan(\omega T_{1\text{e}})]}{\left(1+\omega^2T_{1\text{e}}^2\right)^{b/2}}. \tag{4}$$

The paramagnetic relaxation rate constant $1/T_{1,\text{para}}$ is then proportional to this spectral density [26]:

$$\frac{1}{T_{1,\text{para}}} = M_{2,\text{para}} \cdot J_{\text{para}}(\omega). \tag{5}$$

where $M_{2,\text{para}}$ is the averaged second moment arising from the dipolar coupling of electron and proton nuclear spins. Its value can be expressed via the averaged diamagnetic protein proton second moment of the Eq. (1)

$$M_{2,\text{para}} = \overline{M}_{2\text{H}}C\frac{N_{\text{e}}}{N_{\text{H}}}\frac{S(S+1)}{I(I+1)}\frac{\gamma_{\text{S}}^2}{\gamma_{\text{I}}^2}. \tag{6}$$

Here N_{e} is the number of electron spins in a protein, N_{H} is the number of protein protons and C is a numerical constant that arises due to the structural and dynamical differences of the proton or electron spins that surround the reference spin.

In the high frequency limit, $\omega T_{1\text{e}} \gg 1$, the equation describing the relaxation due to the coupling with the electron spins, Eq. (5), qualitatively coincides with that previously derived, Eq. (1). For this limiting case, Eq. (4) becomes

$$J_{\text{para}}^{\text{lim}}(\omega) = 2\sqrt{\frac{2}{\pi}}\Gamma(b)\tau_{\text{uf}}^{1-b}\frac{\cos\left[b\frac{\pi}{2}\right]}{\omega^b}. \tag{7}$$

Comparing the equivalent reduced spectral density (in square brackets) of Eq. (1) with the reduced spectral density in Eq. (7) one can obtain the value of the characteristic correlation time τ_{uf}

$$\tau_{\text{uf}}^{1-b} = \frac{4\pi d_S\frac{k_{\text{B}}T}{\hbar}\left\{\frac{3}{4}\left(1+\frac{1}{2^b}\right)\Omega_{\parallel}^{b-2} + \frac{1}{6}\left(\frac{7}{2}+\frac{1}{2^b}\right)\Omega_{\perp}^{b-2}\right\}}{2\sqrt{\frac{2}{\pi}}\Gamma(b)\cos\left(b\frac{\pi}{2}\right)}. \tag{8}$$

Substituting Eqs. (4), (6) and (8) into Eq. (5) yields

$$\frac{1}{T_{1,\text{para}}} = 4C\pi d_{\text{S}}\frac{k_{\text{B}}T}{\hbar}\left\{\frac{3}{4}\left(1+\frac{1}{2^b}\right)\Omega_{\parallel}^{b-2} + \frac{1}{6}\left(\frac{7}{2}+\frac{1}{2^b}\right)\Omega_{\perp}^{b-2}\right\} \times \overline{M}_{2\text{H}}\frac{N_{\text{e}}}{N_{\text{H}}}\frac{\gamma_S^2}{\gamma_I^2}T_{1e}^{b}\frac{\cos[b\arctan(\omega T_{1\text{e}})]}{\cos\left(b\frac{\pi}{2}\right)\left(1+\omega^2T_{1\text{e}}^2\right)^{b/2}}. \tag{9}$$

The solid line through the data in Fig. 1 was computed using Eq. (9). At high values of the magnetic field, the field dependence is a power law in the proton Larmor frequency, but at low field strengths corresponding to small Larmor frequencies or long correlation times, the electron–nuclear dipolar coupling is interrupted by the electron spin-lattice relaxation that limits the correlation and causes the plateau. The position of the low-field cut-off provides a measurement of the electron spin–lattice relaxation time, which in the present case is found to be 1.7 μs at fields below approximately 0.2 MHz or 2.3 mT based on Eq. (9). Direct measurements of $T_{1\text{e}}$ at 9.6 GHz using a Bruker pulsed ESR spectrometer yields longitudinal decays that may be biexponential but the dominant $T_{1\text{e}}$ is for these samples of 4–6 μs, which is longer that the value obtained from analysis of the MRD profiles by a factor somewhat larger than 2. The difference in the electron Larmor frequency of these two measurements is nearly a factor of 700. The electron spin relaxation rate constant is generally dependent on magnetic field strength, decreasing with increasing field. Although the dynamics in the lyophilized protein are minimized by the absence of solvent, high frequency motions are expected to persist. At 9.6 GHz, $1/\omega_S = 16$ ps, and it is reasonable that there are local dynamics in this range that cause a dispersion in the electron relaxation rate constant. The present data are insufficient to define the shape of the electron dispersion, we simply note that the difference between the two measurements of the electron relaxation time is not large and in the direction expected for the field dependence of the electron relaxation time constant.

The crucial feature of these data is the very large contribution to the protein proton spin–lattice relaxation rate constant at low magnetic field strengths caused by the covalently bound nitroxide radical, which has a long electron $T_{1\text{e}}$. Below the cut-off frequency of approximately 0.2 MHz, the proton relaxation rate constant is independent of magnetic field strength and proportional to the electron spin–lattice relaxation time. The electron $T_{1\text{e}}$ of several microseconds is much longer than the values usually found for metal-based contrast agents, which are in the range of hundreds or tens of picoseconds. Therefore, the magnitude of the paramagnetic contribution to the ^1H_2O spin–lattice relaxation is increased in proportion to the increase in the electron-spin $T_{1\text{e}}$ values.

In the present experiments, the nitroxide radical has a single unpaired electron, i.e. $S = 1/2$. The relaxation rate constant, $1/T_{1,\text{para}}$, is proportional to the second moment that arises due to the coupling of a reference proton spin with an electron spin and, therefore, is the function of $S(S+1)$ [28]. Compared with metal systems such as gadolinium(III) ion, $S = 7/2$, or Mn(II), $S = 5/2$, the value of $S(S+1)$ is smaller for the nitroxide systems by a factor of 21 and 11.67, respectively. Nevertheless, the much longer electron relaxation time for the nitroxide radical compared with the metals ions makes the low field relaxation efficiency of the nitroxide labeled BSA much larger than for the protein covalently labeled with metal-chelates [14]. The magnitude of the paramagnetic contribution to the proton relaxation rate constant is large enough to be competitive for applications as magnetic contrast agents

provided that the long electron T_{1e} is maintained in the target environment and the exchange of rare long-lived water molecules provides a coupling mechanism to carry the efficient proton relaxation to the solvent protons.

The electron spin–lattice relaxation time is a function of the local dynamics of the nitroxide that may modulate the nitroxide anisotropic g-tensor or hyperfine tensor. Therefore, local dynamical constraint of the spin label is important and is accomplished for the data in Fig. 1 by eliminating the solvent. Fig. 2 shows the water proton spin-lattice relaxation dispersion profile for the spin-labeled protein cross-linked as a gel, which is a good model for a tissue labeled with a targeted contrast agent. The detected spins are now the water protons that completely dominate the intensity of the proton NMR signal. The water–proton MRD profile is similar to that of the dry protein except that the onset of the low field plateau is shifted to higher Larmor frequency corresponding to an electron T_{1e} of 0.10 μs and the low-field relaxation rate is consequently smaller. This result demonstrates the importance of the nature of the chemical coupling between the radical and the macromolecular matrix. In the present case, the flexibility afforded by the addition of excess solvent in the protein coupled spin label shifts the electron T_{1e} by more than a factor of 10.

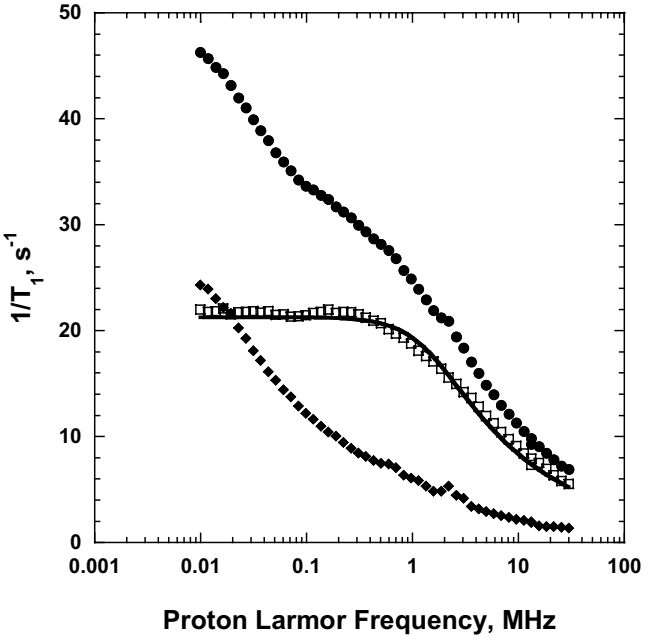

Fig. 2. The water–proton spin–lattice relaxation rate constant for a cross-linked 15% gel of bovine serum albumin covalently labeled with 0.6 equivalents of iodoacetamido-PROXYL spin label as a function of the magnetic field strength reported as the proton Larmor frequency. (●) the total relaxation rate for the paramagnetic protein; (♦) the relaxation rate constants for the unlabeled 15% diamagnetic protein gel; (□) the paramagnetic relaxation rate contribution obtained by subtraction of the diamagnetic relaxation rate constants from the total relaxation rate constants. Data were obtained at 302 K. The solid line represents a best fit to Eq. (9) with the parameters $T_{1e} = 0.10$ μs, $b = 0.42$, and $D = 1.7 \times 10^4$ $(s^{-1})^{b+1}$, where $D = 4\,C\pi d_S \frac{k_B T}{\hbar}\left\{\frac{3}{4}\left(1+\frac{1}{2^b}\right)\Omega_{\|}^{b-2} + \frac{1}{6}\left(\frac{7}{2}+\frac{1}{2^b}\right)\Omega_{\perp}^{b-2}\right\}\overline{M}_{2H}\frac{N_e}{N_H}\frac{\gamma_S^2}{\gamma_I^2}$.

We may understand the water proton relaxation profile in Fig. 2 based on that for the protein protons shown in Fig. 1. The nitroxide electron spin may relax the protein protons efficiently by direct electron–nuclear dipolar couplings. The proton spin–spin coupling in the non-rotating protein is efficient so that the protein spins thermalize rapidly compared with the protein–proton spin-lattice relaxation time. The relatively few water molecules that bind to the protein in long-lived sites, i.e. in the range from 100 ns to 10 μs, are also strongly coupled with the surrounding protein protons and rapidly come to spin equilibrium with the protein protons. The result is efficient relaxation of the protein-bound water proton population. Labile exchange of the protein-bound water molecules with the bulk carries the relaxation effects, including the field dependence of the paramagnetic protein protons, to the water population as a whole with the usual dilution caused by the large difference in the proton population in the water compared with the protein. We note that a limitation in the magnetization transfer rate between the paramagnetic solid and the water pool may also cause a plateau in the relaxation profile, which is observed at very low frequencies in hydrated protein systems [18–20]. However, the limitation observed in the present experiments is at much higher frequency and lower rates, which supports the conclusion that the plateau is correctly described as the limitation by the electron relaxation rate.

It is well known that there is a direct effect of the nitroxide electron spin on the diffusing water spins that has been discussed in detail elsewhere [16,17]. The direct electron–nuclear coupling modulated by translational diffusion, which is dominated by the rapid motion of the water spins, is well characterized, has a different magnetic field dependence, and provides a much smaller contribution to the water spin–lattice relaxation than found here [16,17]. The low field relaxivity associated with the nitroxide bound to a freely rotating and diffusing protein in solution is approximately 1 s^{-1} mM^{-1}. Dividing paramagnetic contribution to the relaxation rate constant by the nitroxide concentration in the gel sample in Fig. 2 yields a much larger low field relaxivity of 16.1 s^{-1} mM^{-1}, clearly dominant compared with the diffusional contribution.

The electron T_{1e} in the gel system is approximately 10 times shorter than in the dry protein. The complete hydration of the system in a cross-linked gel changes the structure of the protein somewhat and the proton second moment changes in response [24]. The fully hydrated system permits protein side chain motion in the system including motion of the covalently attached nitroxide spin label that modulates the electron spin energy because the g and hyperfine tensors are anisotropic. Therefore, it is expected that the electron T_{1e} should decrease in the gel relative to the lyophilized and more rigid solid.

The value of b deduced from the data in Fig. 2 for the paramagnetic contribution to the proton relaxation in the gel system is 0.42, which is small compared with values obtained from diamagnetic systems. As noted above, b is a

function of the spectral dimension, d_s, and the fractal distribution of protons, d_f. Both of these parameters may be different for the paramagnetic contribution compared with the diamagnetic contribution because the electron center establishes a unique reference point from which the fractal distribution of protons is computed. The result may be different from the average d_f when a number of reference origins are taken as is appropriate for the proton relaxation case. The spectral or fraction dimension, d_s, describes the dimensionality appropriate to the propagation of the structural disturbance that modulates the dipolar couplings in the system. For the paramagnetic contribution, this includes both the motion of the protons in the field of the electron spin that is driven by the chain dynamics and the motion of the electron moment on the attachment tether in the fully hydrated gel case. Although this representation of the theory does not explicitly include effects of local motion of the electron moment that is independent of the chain, the expectation is the effect is to smear the location of the electron moment and increase the value of d_s. If we fix the value of d_f at 2.5 then the value of d_s that yields 0.42 for b is 1.43, which is 7% larger than that we have found for the diamagnetic protein systems studied to date. We wish to make it clear that this discussion of the parameters d_f and d_s for the paramagnetic contribution are speculative; however, the magnitudes appear to be quite reasonable.

4. Conclusion

The rotational immobilization of organic radicals with long electron spin–lattice relaxation times in protein or other macromolecular proton-rich systems provides an opportunity to influence water proton relaxation rates very significantly at low magnetic field strengths. When normalized to the spin concentration, the relaxation efficiency may be greater than for corresponding metal chelate systems. In addition, the high field portion of the relaxation dispersion, which is a power law in the Larmor frequency, may provide a very useful report of higher frequency internal motions in the protein that are not directly accessible in diamagnetic rotationally immobilized systems.

Acknowledgments

This work was supported by the National Institutes of Health, the University of Virginia, USA and the CNRS, France.

References

[1] S. Aime et al., Gd(III) based contrast agents for MRI, Adv. Inorg. Chem. 57 (2005) (Chapter 4).
[2] S. Aime, A. Barge, E. Gianolio, R. Pagliarin, L. Silengo, L. Tei, High relaxivity contrast agents for MRI and molecular imaging, Ernst Schering Research Foundation Workshop 49 (2005) 99–121.
[3] R.N. Muller, L. Vander Elft, A. Roch, J.A. Peters, E. Csajbok, P. Gillis, Y. Gossuin, Relaxation by metal-containing nano systems, Adv. Inorg. Chem. 57 (2005) 71–83.
[4] S. Aime, E. Gianolio, D. Longo, R. Pagliarin, C. Lovazzano, M. Sisti, New insights for pursuing high relaxivity MRI agents from modelling the binding interaction of Gd(III) chelates to HSA, Chembiochemistry 6 (2005) 818–820.
[5] E. Belorizky, P.H. Fries, Simple analytical approximation of the longitudinal electronic relaxation rate of Gd(III) complexes in solutions, Phys. Chem. Chem. Phys. 6 (2004) 2341–2351.
[6] I. Bertini, C. Luchinat, NMR of Paramagnetic Molecules in Biological Systems, Benjamin/Cummings:, Menlo Park, CA, 1986.
[7] K.E. Kellar, P.M. Henrichs, R. Hollister, S.H. Koenig, J. Eck, D. Wei, High relaxivity linear Gd(DTPA)-polymer conjugates: the role of hydrophobic interactions, Magn. Reson. Med. 38 (1997) 712–716.
[8] S.H. Koenig, From the relaxivity of Gd(DTPA)2- to everything else, Magn. Reson. Med. 22 (1991) 183–190.
[9] S.H. Koenig, Classes of hydration sites at protein–water interfaces: the source of contrast in magnetic resonance imaging, Biophys. J. 69 (1995) 593–603.
[10] S.H. Koenig, K.E. Kellar, Theory of 1/T1 and 1/T2 NMRD profiles of solutions of magnetic nanoparticles, Magn. Reson. Med. 34 (1995) 227–233.
[11] S.H. Koenig, K.E. Kellar, Blood-pool contrast agents for MRI: a critical evaluation, Acad. Radiol. 5 (Suppl 1) (1998) S200–S205, discussion S226-207.
[12] S. Aime, A. Barge, C. Cabella, S.G. Crich, E. Gianolio, Targeting cells with MR imaging probes based on paramagnetic Gd(III) chelates, Curr. Pharm. Biotechnol. 5 (2004) 509–518.
[13] L. Frullano, J. Rohovec, S. Aime, T. Maschmeyer, M.I. Prata, J.J. de Lima, C.F. Geraldes, J.A. Peters, Towards targeted MRI: new MRI contrast agents for sialic acid detection, Chemistry 10 (2004) 5205–5217.
[14] J.P. Korb, G. Diakova, R.G. Bryant, Paramagnetic Relaxation of Protons in Rotationally Immobilized Proteins, J. Chem. Phys. 124 (2006) 134910–134916.
[15] M.W. Hodges, D.S. Cafiso, C.F. Polnaszek, C.C. Lester, R.G. Bryant, Water translational motion at the bilayer interface: an NMR relaxation dispersion measurement, Biophys. J. 73 (1997) 2575–2579.
[16] C.F. Polnaszek, R.G. Bryant, Self diffusion of water at the protein surface: a measurement, J. Amer. Chem. Soc. 106 (1984) 428–429.
[17] C.F. Polnaszek, R.G. Bryant, Nitroxide radical induced solvent proton relaxation: measurement of localized translational diffusion, J. Chem. Phys. 81 (1984) 4038–4045.
[18] J.P. Korb, R.G. Bryant, The physical basis for the magnetic field dependence of proton spin–lattice relaxation rates in proteins, J. Chem. Phys. 115 (2001) 10964–10974.
[19] J.P. Korb, R.G. Bryant, Magnetic field dependence of proton spin–lattice relaxation times, Magn. Reson. Med. 48 (2002) 21–26.
[20] J.P. Korb, R.G. Bryant, Magnetic field dependence of proton spin–lattice relaxation of confined proteins, C.R. Phys. 5 (2004) 349–357.
[21] J.P. Korb, A. Van-Quynh, R.G. Bryant, Proton spin relaxation induced by localized spin–dynamical coupling in proteins, Chem. Phys. Lett. 339 (2001) 77–82.
[22] D.A. Mendelson, J.F. Heinsbergen, S.D. Kennedy, L.S. Szczepaniak, C.C. Lester, R.G. Bryant, Comparison of agarose and cross-linked protein gels as magnetic resonance imaging phantoms, Magn. Reson. Imaging 9 (1991) 975–978.
[23] R. Kimmich, W. Nusser, F. Winter, In vivo NMR field-cycling relaxation spectroscopy reveals 14N1H relaxation sinks in the backbones of proteins, Phys. Med. Biol. 29 (1984) 593–596.
[24] Y. Goddard, J.P. Korb, R.G. Bryant, Structural and dynamical examination of the low-temperature glass transition in serum albumin, Biophys. J. 91 (2006) 3841–3847.
[25] T. Miyazawa, T. Shimanouchi, S. Mizushima, Normal vibrations of *N*-methyl acetamide, J. Chem. Phys. 29 (1958) 611–616.
[26] A. Abragam, The Priniciples of Nuclear Magnetism, The Clarendon Press, Oxford University Press, Oxford, 1961 (Chapter 8).
[27] G. Lipari, A. Szabo, Model-free approach to the interpretation of nuclear magnetic resonance relaxation in macromolecules. 1. Theory and range of validity, J. Am. Chem. Soc. 104 (1982) 4546–4559.
[28] C.P. Slichter, Principles of Magnetic Resonance, 3rd ed., Springer, Berlin, Heidelberg, New York, 1980.